JOURNAL OF GEOPHYSICAL RESEARCH, VOL. 114, D24109, doi:10.1029/2009JD012493, 2009

Evaluation of AIRS, IASI, and OMI ozone profile retrievals in the extratropical tropopause region using in situ aircraft measurements

Jasna V. Pittman,[1] Laura L. Pan,[1] Jennifer C. Wei,[2] Fredrick W. Irion,[3] Xiong Liu,[4,5] Eric S. Maddy,[2] Christopher D. Barnet,[6] Kelly Chance,[5] and Ru-Shan Gao[7]

Received 15 May 2009; revised 4 September 2009; accepted 16 September 2009; published 31 December 2009.

[1] We evaluate ozone profile retrievals from the Atmospheric Infrared Sounder (AIRS), the Infrared Atmospheric Sounding Interferometer (IASI), and the Ozone Monitoring Instrument (OMI) using in situ measurements collected on board the NSF/NCAR Gulfstream-V aircraft during the Stratosphere-Troposphere Analyses of Regional Transport 2008 (START08) experiment. The focus of this study is to examine how well the satellite retrieval products capture the ozone gradients and variability in the extratropical upper troposphere lower stratosphere (UTLS). The AIRS retrieval examined is version 5, while IASI and OMI retrievals are research products. All satellite instruments show excellent ability in capturing synoptic-scale ozone gradients associated with strong potential vorticity (PV) gradients. The positive ozone-PV correlation near the tropopause is also well represented in the satellite data in comparison to collocated aircraft measurements. During aircraft cruise legs, more than 90% of collocated satellite retrievals agree with aircraft measurements within ±50% for ozone mixing ratios greater than 200 ppbv. Below 200 ppbv, AIRS and IASI retrievals show significant positive biases, while OMI shows both positive and negative biases. Ozone gradients across the tropopause are well-captured, with median values within 30% (positive for AIRS and IASI, negative for OMI) and variances within ±50%. Ozone variability in the UTLS is captured by the satellite retrievals at the 80% level. In the presence of high clouds, however, the infrared retrievals show the largest positive biases. Despite the limited vertical information content, the high horizontal coverage and long-term data availability make these satellite data sets a valuable asset for UTLS research.

Citation: Pittman, J. V., L. L. Pan, J. C. Wei, F. W. Irion, X. Liu, E. S. Maddy, C. D. Barnet, K. Chance, and R.-S. Gao (2009), Evaluation of AIRS, IASI, and OMI ozone profile retrievals in the extratropical tropopause region using in situ aircraft measurements, *J. Geophys. Res.*, *114*, D24109, doi:10.1029/2009JD012493.

1. Introduction

[2] The upper troposphere and lower stratosphere (UTLS) is a region of the atmosphere where chemistry, dynamics, radiation, and climate are highly coupled. This region contains the tropopause, a boundary that separates the chemically and dynamically distinctive troposphere from the stratosphere. Among some outstanding issues that exist in UTLS research are the understanding of the chemical and dynamical processes that control the concentration of water vapor and ozone. These processes give rise to the large gradients in water vapor and ozone found across the tropopause. Changes in the gradients of these two tracers have a direct impact on the radiative balance of the tropopause region, which in turn influences exchange of air between the UT and the LS [*Gettelman et al.*, 2004]. In addition to water vapor and ozone, questions on the radiative impact of near-tropopause clouds and the role that aerosols injected by deep convection play on cloud formation also remain important topics of investigation. Ultimately, our improved understanding of the chemical and dynamical processes affecting the composition of the UTLS will enhance our regional and global modeling capabilities and thus provide more accurate forecasts of changes in the climate system.

[3] The concentration and distribution of UTLS water vapor and ozone are sensitive to both chemical processes, such as cloud microphysics, and transport processes, such as

[1]National Center for Atmospheric Research, Boulder, Colorado, USA.
[2]Perot Systems Government Services, Fairfax, Virginia, USA.
[3]Jet Propulsion Laboratory, California Institute of Technology, Pasadena, California, USA.
[4]Goddard Earth Sciences and Technology Center, University of Maryland Baltimore County, Baltimore, Maryland, USA.
[5]Harvard-Smithsonian Center for Astrophysics, Cambridge, Massachusetts, USA.
[6]Center for Satellite Application and Research, National Environmental Satellite, Data, and Information Service, NOAA, Camp Springs, Maryland, USA.
[7]National Oceanographic and Atmospheric Administration, Boulder, Colorado, USA.

0148-0227/09/2009JD012493$09.00

convection and stratosphere-troposphere exchange (STE) [*Holton et al.*, 1995]. These processes can have a direct effect on climate. For instance, increases in UTLS ozone can contribute to a warming of the tropopause, which allows higher water vapor concentrations to enter the stratosphere [*Xie et al.*, 2008]. Higher stratospheric water vapor coupled with stratospheric cooling induced by increases in atmospheric carbon dioxide can lead to increases in stratospheric ozone depletion, in particular in the Arctic where temperatures in the vortex reside close to threshold for cloud formation and are thus highly dependent on water vapor concentrations [*Kirk-Davidoff et al.*, 1999]. Changes in stratospheric ozone then affect both the tropospheric ozone budget and the amount of harmful ultraviolet (UV) rays reaching Earth's surface.

[4] UTLS ozone is of particular interest because global ozonesonde measurements have shown this layer to have the largest negative trends, with the largest losses happening in the Northern Hemisphere midlatitudes during the spring [*Logan et al.*, 1999]. The dominant processes responsible for these trends, whether it is transport (e.g., downward transport from the stratosphere and upward transport of boundary layer air by convection) and/or chemistry (e.g., heterogeneous reactions on the surface of cirrus clouds [*Smith et al.*, 2001]), remain under investigation.

[5] Observations of UTLS ozone on a daily and global basis have been limited. Motivated by the need of UTLS ozone information for investigating UTLS composition and links to climate, we examine the quality of several newly available UTLS ozone satellite data sets. The large gradient across the tropopause and the large spatial variability associated with weather patterns pose significant challenges to satellite instruments. Thus the main objective of this work is to examine, from a data user's perspective, how well current satellite retrieval products capture the ozone gradients and variability in the extratropical UTLS, between 100 and 300 hPa. We accomplish this goal by comparing the satellite ozone retrievals to the "true" conditions represented by in situ aircraft measurements of ozone obtained during a recent field campaign. While this study does not focus on the details of the retrieval algorithms, the results presented, however, should help characterize the sensitivity of satellite instruments retrieving ozone in the UTLS, provide data users a better understanding of the capabilities and limitations of the satellite data sets, and provide satellite instrument science teams more information on where improvements to the retrieval algorithms are needed.

[6] Three satellite data sets are examined in this study. These particular data sets are chosen because they provide vertical profile information as well as wide horizontal sampling. The first data set is obtained from the Atmospheric Infrared Sounder (AIRS) on NASA's EOS-Aqua satellite, the instrument with the longest UTLS ozone record of all the space-borne observations considered in this study. AIRS has been operating successfully since 2002 [*Aumann et al.*, 2003]. It was designed to primarily measure atmospheric profiles of temperature and water vapor; however, its spectral coverage also contains information on trace gases such as ozone, carbon dioxide, carbon monoxide, and methane [e.g., *Bian et al.*, 2007; *Maddy et al.*, 2008; *Chahine et al.*, 2008; *Yurganov et al.*, 2008; *McMillan et al.*, 2005; *Xiong et al.*, 2008, 2009]. The retrieval accuracy of temperature and water depends in part on the retrieval of these trace gas products. Consequently, we seek to explore the information content of one of these trace gas products, ozone in our case, and the potential contribution this product can have on UTLS chemistry and transport research. Previous studies using earlier versions of AIRS ozone have shown the retrievals can reproduce the gradients and variability of ozone in the UTLS region [*Bian et al.*, 2007; *Monahan et al.*, 2007; *Pan et al.*, 2007]. Vertical profiles using the latest retrieval algorithm, Version 5 (V5), have been examined against ozonesondes [*Divakarla et al.*, 2008]. The performance of V5 retrievals in the UTLS, however, has not been investigated. Therefore this study provides the first opportunity to examine how V5 profile retrievals in the UTLS capture gradients and variability in ozone using aircraft measurements where both horizontal (e.g., constant pressure) and vertical (e.g., ascent and descent) flight tracks are available.

[7] The second satellite data set is obtained from the recently launched Infrared Atmospheric Sounding Interferometer (IASI) instrument on EUMETSAT's MetOp-A satellite. Given the similarities of the AIRS and IASI instruments, the IASI retrievals examined here are a research product that currently uses the same algorithm and first guess as AIRS. IASI on MetOp-A is the first in a series of three identical infrared interferometers planned to provide over 15 continuous years of data. Therefore it is crucial to characterize the IASI retrievals in order to establish the accuracy of what promises to be an unprecedented long data record for an infrared sounder.

[8] The third satellite data set is obtained from the Ozone Monitoring Instrument (OMI) on NASA's EOS-Aura satellite. Contrary to AIRS and IASI, OMI is a UV/Visible instrument specifically designed to measure ozone. OMI inherited the advantages of the well-established and well-characterized Global Ozone Monitoring Experiment (GOME), the Scanning Imaging Absorption Spectrometer for Atmospheric Cartography (SCHIAMACHY), and the Total Ozone Mapping Spectrometer (TOMS) instruments, which have been making ozone measurements since 1978. This study examines a new research product, OMI vertical profile retrievals.

[9] A significant strength of these three satellite instruments is their high horizontal sampling coverage. This wide coverage can provide large-scale context for in situ measurements as well as establish the relationship between large-scale ozone features and meteorological fields in the UTLS region. The wide coverage achieved by these nadir-viewing instruments, however, comes at the expense of coarser vertical resolution. Limb-viewing instruments, such as the Microwave Limb Sounder (MLS) on Aura, provide a higher vertical resolution but have a limited spatial coverage and a coarse horizontal resolution. Ultimately, research efforts would benefit from a unified data set capable of describing both vertical and horizontal structures as well as total columns of ozone by combining the strengths of each contributing measurement. The success of such unified data set, however, depends on the proper characterization and validation of each contributing retrieval.

[10] The in situ aircraft data presented in this study are from the Stratosphere-Troposphere Analyses of Regional Transport 2008 (START08) experiment [*Pan et al.*, 2009]

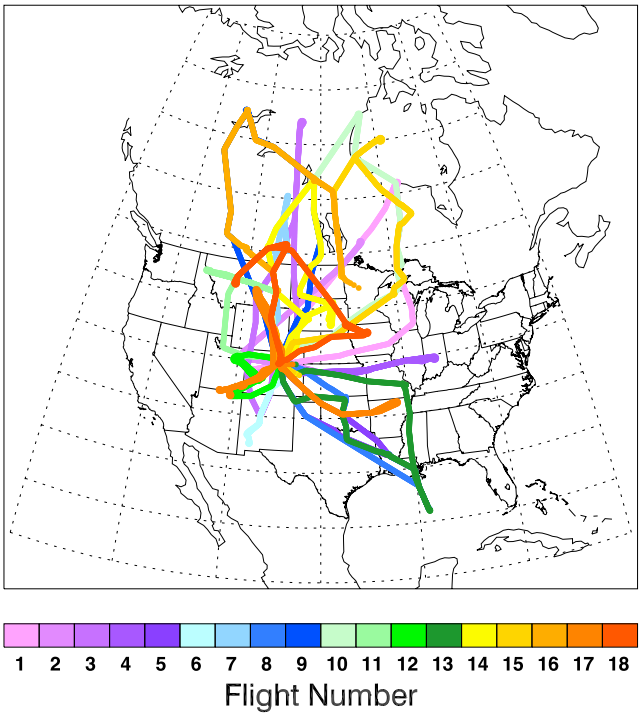

Figure 1. Geographical coverage of all 18 research flights during the START08 campaign.

(for more information on the campaign, visit http://www.acd. ucar.edu/start/). This campaign was designed to study transport pathways in the extratropical UTLS and to investigate the behavior of the extratropical tropopause. The NSF/NCAR Gulfstream-V aircraft (GV) was the measuring platform used, and it sampled a large portion of the North American continent (25° to 63°N, 86° to 117°W) between April and June 2008. A total of 18 research flights were completed covering heights from the surface up to 130 hPa (or ~14.4 km). The GV ground tracks for all 18 flights are shown in Figure 1.

[11] This paper is structured as follows. Section 2 presents a description of the data sets used. Section 3 describes the methodology used to address the different spatial and temporal resolutions of the data sets examined. Section 4 explores how well the satellite data sets can capture dynamic variability of ozone on a synoptic scale over North America, gradients and variability of ozone during constant pressure flight tracks, troposphere-to-stratosphere ozone gradients, and ozone-potential vorticity (PV) correlations in the UTLS. The latter analysis provides a good comparison for how aircraft and satellite ozone respond to the dynamic changes represented in PV space. Section 5 provides a summary of our findings.

2. Data

2.1. Aircraft Measurements of Ozone

[12] Two sets of high-rate (1 Hz) measurements of ozone were performed aboard the GV aircraft during the START08 campaign: one by the NCAR fast-ozone instrument and the other by the NOAA dual beam UV absorption photometer. For the purpose of this study, the two data sets are equivalent, so we use only the NOAA ozone data in subsequent discussions. The NOAA instrument detects ambient ozone by direct absorption at 254 nm [*Proffitt and McLaughlin*, 1983]. Ozone is measured using two identical chambers where one analyzes ambient air and the other one analyzes ozone-scrubbed air. Ozone number density is then calculated using ozone's absorption cross section at 254 nm and the Beer-Lambert Law. The accuracy of the measurement is ±3% with a precision of 1.5×10^{10} molecules/cm^3. The START08 campaign targeted different transport processes that affect the extratropical UTLS, namely tropospheric intrusions, stratospheric intrusions or tropopause folds, and convection [*Pan et al.*, 2009]. Figure 2 shows the sampling frequency of ozone as a function of height. Note the frequent and large variability observed between 100 and 300 hPa. These profiles are evidence of the impact that different dynamical regimes can have on the chemical composition of the UTLS.

2.2. Satellite Measurements of Ozone

2.2.1. AIRS

[13] AIRS is a cross-track scanning hyperspectral grating spectrometer on board NASA's EOS-Aqua satellite, launched in May 2002. The satellite flies in a polar Sun-synchronous orbit that crosses the equator at 0130 (descending) and 1330 (ascending) local time. AIRS has 2378 spectral bands in the infrared (IR) covering from 3.7 to 15.4 μm (with gaps) at a spectral resolution of ~0.5 cm^{-1}. The horizontal resolution is 13.5 km at nadir in level 1, and the horizontal sampling extends up to ±1650 km from nadir, providing global coverage twice a day.

[14] Retrievals in the presence of clouds are done with the help of the Atmospheric Microwave Sounding Unit-A (AMSU-A), also on board Aqua. The resulting cloud-cleared radiances for AIRS using microwave observations are obtained at a horizontal resolution determined by a single AMSU-A footprint, or field of regard (FOR), which coincides with nine AIRS fields of view (FOV). The AMSU-A footprint sets the AIRS level 2 horizontal resolution at ~45 km.

[15] In this study, we use V5, level 2, 100-level support product data files provided by the NASA Goddard Earth Sciences Data and Information Services Center (DISC). The ozone retrieval algorithm used in V5 is based on the constrained minimum variance method [*Chahine*, 1968]. A description of the algorithm and the details of the cloud-clearing methodology are given by *Susskind et al.* [2003]. Briefly, the atmospheric temperature profile, water profile, surface temperature, and surface emissivity are first obtained from various channels. This information and a first-guess ozone profile are used as inputs to a forward model [*Strow et al.*, 2003]. The difference between the cloud-cleared radiances and the calculated radiances from the forward model is then minimized using the singular value decomposition technique.

[16] The first-guess ozone profile used in V5 is based on a 15-year climatology of ozonesondes and SAGE data, and it varies as a function of month, latitude, and altitude [*McPeters et al.*, 2007]. This first guess differs significantly from the previous version, V4, which uses regression retrievals from selected days of global ECMWF analyses. A detailed study comparing V4 and V5 of AIRS ozone is presented by *Divakarla et al.* [2008].

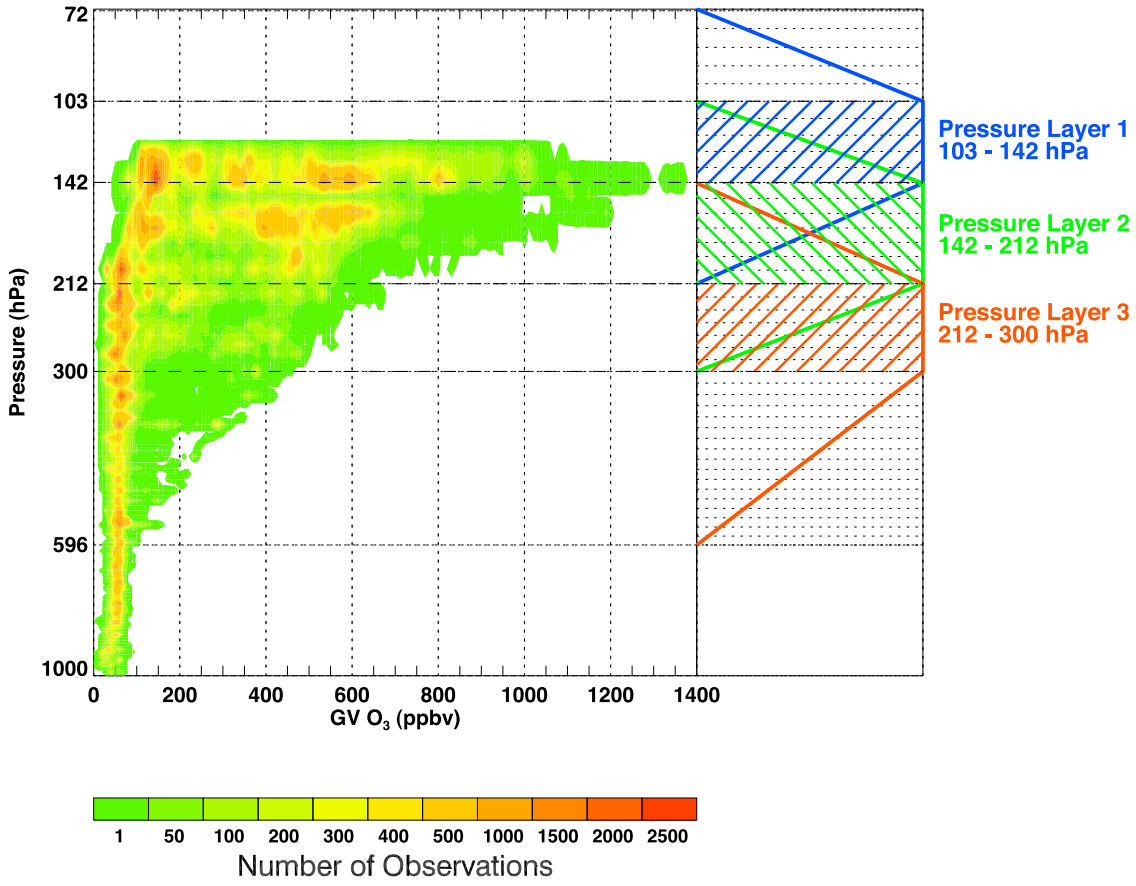

Figure 2. Two-dimensional frequency plot of vertical profiles of aircraft measurements of ozone collected during START08. This study focuses on the 100–300 hPa region where measurements show the largest variability in ozone. To the right of the profile is a schematic of the three basis functions from the AIRS V5 retrievals found in the UTLS region, the pressure levels from the 100-level support product, and the pressure layers (diagonal hatched areas) used in this study.

[17] The V5 ozone retrieval is based on 41 channels around the 9.6 μm ozone band. Over midlatitudes, the total degrees of freedom (DOF) in the vertical are 1.1–2.5, with values of 0.8–2.0 in the stratosphere and 0.1–0.8 in the troposphere. The instrument's sensitivity shows a primary peak between 20 and 30 km and a secondary peak in the lower troposphere, below 10 km (J. C. Wei et al., Ozone profile retrieval experiments using tropopause-based climatology and optimal estimation approach, submitted to *Journal of Atmospheric and Oceanic Technology*, 2009). For more details on the vertical resolution of the V5 retrievals, see the work of *Maddy and Barnet* [2008].

[18] Vertical profiles of ozone are initially derived using a linear combination of nine retrieval basis functions, each one occupying a different pressure range. Three of those nine basis functions are located in the UTLS region, between 100 and 300 hPa. A schematic of the UTLS retrieval basis functions and the pressure levels from the 100-level support product is shown in Figure 2.

[19] In this study, we evaluate the latest (i.e., V5) AIRS ozone product available. However, optimization of the ozone profile retrieval, including retrieval method and a priori climatology, continues to be a topic of research (J. C. Wei et al., submitted manuscript, 2009).

2.2.2. IASI

[20] IASI is a cross-track scanning hyperspectral Michelson Interferometer [*Clerbaux et al.*, 2007] on board EUMETSAT's MetOp-A satellite, launched in October 2006. The satellite flies in a polar Sun-synchronous orbit that crosses the equator at 0930 (descending) and 2130 (ascending) local time. As previously mentioned, plans exist to launch the same instrument on MetOp-B in 2012 and on MetOp-C in 2016. IASI has 8461 spectral bands in the IR covering from 3.7 to 15.4 μm at a spectral resolution of $\sim$0.35 cm^{-1}, higher than AIRS. The Level 1 horizontal resolution is 12 km at nadir, and the horizontal sampling extends up to $\pm$1100 km from nadir, providing global coverage twice a day.

[21] IASI also requires microwave observations for cloud-clearing purposes. To this end, AMSU-A, on board MetOp-A, is used. Similar to the instrument on board Aqua, this AMSU-A has a footprint of $\sim$45 km, which sets the horizontal resolution for the IASI Level 2 ozone product. There are only four collocated IASI FOVs within a single AMSU-A FOR. Cloud clearing from IASI is more challenging, since there are fewer observations of the scene (i.e., fewer FOVs), and a minimum cloud contrast, or variance among all FOVs per FOR, still has to be met for a profile to be accepted.

[22] In this study, we use level 2 IASI ozone retrievals produced as a research product by the NOAA National Environmental Satellite, Data, and Information Service (NESDIS) Center for Satellite Application and Research (STAR). The IASI ozone retrieval uses 53 channels also within the 9.6 μm spectral region. Over midlatitudes, the total DOFs are 1.3–2.7, with values of 0.8–2.2 in the stratosphere and 0.2–1.1 in the troposphere.

[23] The IASI product evaluated in this study uses the AIRS retrieval algorithm and the *McPeters et al.* [2007] ozone climatology as a first guess. This research product was fully operational after September 2008. For the START08 campaign (April–June 2008), however, IASI data were not produced with an algorithm that was optimized to the best of the instrument's performance. While the AIRS algorithm used for IASI has had almost 7 years of optimization and comparison with in situ, ground, and other satellite data, efforts to develop an independent IASI ozone algorithm are ongoing.

2.2.3. OMI

[24] OMI is a nadir-viewing pushbroom instrument on board NASA's Aura satellite, launched in July 2004. Aura also flies in a polar Sun-synchronous orbit. Up until November 2007, Aura had a 0145 equator-crossing time, about a 15-min separation with Aqua. As of 8 May 2008, Aura trails Aqua by 7–8 min. OMI measures backscattered hyperspectral radiances in the UV/visible range of 270–500 nm in three channels (UV-1: 270–310 nm, UV-2: 310–365 nm, visible: 350–500 nm) at spectral resolution of 0.42–0.63 nm [*Levelt et al.*, 2006]. The horizontal resolution is 13 km × 48 km for UV-1 and 13 km × 24 km for UV-2 and visible channels at nadir, and its horizontal sampling extends up to ±1300 km from nadir, providing global coverage once a day.

[25] This study uses a new research product derived from the 270–330 nm UV radiances. This product provides profiles of partial ozone columns retrieved at 24 layers from the surface to ~60 km using the optimal estimation technique. The a priori information, both mean profile and its standard deviation, used in the retrievals is based on the *McPeters et al.* [2007] climatology. The total DOFs for signal are ~6.0–7.0, with values of 5.0–6.7 in the stratosphere and 0–1.5 in the troposphere [*Liu et al.*, 2005, 2009]. Validation of this new product against the Microwave Limb Sounder (MLS), also on board the Aura satellite, is currently in progress [*Liu et al.*, 2009].

[26] Clouds in OMI's retrieval are treated as mixed Lambertian surfaces. Cloud top pressure is taken from the OMI O_2-O_2 algorithm [*Acarreta et al.*, 2004] and cloud fraction is fitted as auxiliary parameter in the retrievals. Note that cloud top pressures retrieved from OMI are not the same as the cloud top pressures retrieved from IR measurements but are usually near the midlevel of the cloud due to photon penetration inside the clouds [*Vasilkov et al.*, 2008; *Sneep et al.*, 2008].

[27] To facilitate comparisons with the aircraft and the IR satellite retrievals, level 2 OMI retrievals are interpolated to the 100 vertical levels in AIRS and converted to mixing ratio. Assume D_i is the partial ozone column in Dobson units at layer i (i = 1, 24). From D, we can derive C, the cumulative ozone column at level i, (i.e., the ozone column from top-of-the-atmosphere to a particular pressure level P_i). This cumulative ozone profile is then interpolated through cubic spline to the AIRS 100 pressure levels from the support product used in this analysis to get the profile at the AIRS pressure grid; ozone columns at the original OMI grid are conserved in the interpolation. We then calculate the partial ozone column at each AIRS layer, i.e., D_j (j = 1, 100). For further convenience, OMI data are horizontally mapped onto 0.5° longitude × 0.5° latitude grid cells using an area-weighted tessellation algorithm [*Spurr*, 2003].

2.3. Global Meteorological Analyses Data

[28] Meteorological data used in this study are from the National Center for Environmental Prediction (NCEP) Global Forecast System (GFS) operational analysis. The highest resolution output (T283) was used as part of the START08 forecast and analyses. The data sets are available four times daily on a 0.3125° × 0.3125° global grid (35 km) with 47 pressure levels from 1000 to 1 hPa. The vertical resolution of the data in the UTLS region is ~500 m. PV used in this study is calculated from the temperature and wind data. We also use the GFS tropopause height in the data analysis. In the presence of multiple tropopauses, the first tropopause is considered. More information on the data sets can be found online at http://www.emc.ncep.noaa.gov/gc_wmb/Documentation/TPBoct05/T382.TPB.FINAL.htm.

3. Methodology

[29] The 18 flight dates during the START08 campaign were 18, 21, 24, 28, and 30 April; 1, 4, 6, 9, 12, 14, and 15 May; 16, 18, 23, 24, 26, and 27 June, all in 2008. Their geographical coverage is shown in Figure 1. Data are available for all these days for AIRS and OMI. IASI data are available for all flights except for 4 May (flight 7) and 24 June (flight 16) when no quality-controlled profiles matched the aircraft's geographical coverage.

[30] The focus of this study is the extratropical UTLS region, from ~100 to 300 hPa. This is the region of largest ozone gradient and also the most frequently sampled layer during the START08 campaign (see Figure 2).

[31] The satellite data are evaluated in three pressure layers, coincident with the retrieval basis functions in the UTLS. These layers are bounded by the 103, 142, 212, and 300 hPa pressure levels. We calculate a pressure-weighted average of ozone using the pressure levels that fall within each coarse pressure layer. Figure 2 illustrates the retrieval basis functions, the pressure layers considered in the analysis, and the START08 ozone data distribution.

[32] The in situ aircraft data represent very different spatial scales compared to the satellite measurements. The data we use were reported at a 1-s rate representing ~220 m of horizontal scale. For data evaluation in comparable spatial scales, the aircraft data are averaged to a ~45 km scale during constant pressure flight segments to match the horizontal resolution of the AIRS and IASI Level 2 retrievals. In the vertical, the aircraft measurements are averaged to the three satellite pressure layers described above. The maximum altitude attained during START08 was 14.4 km or 132 hPa. Thus the top pressure layer, with a depth of 450 m, was only partially sampled by the aircraft. This is a limitation of the aircraft data set used in this study that should be kept in mind. The maximum depths of the middle

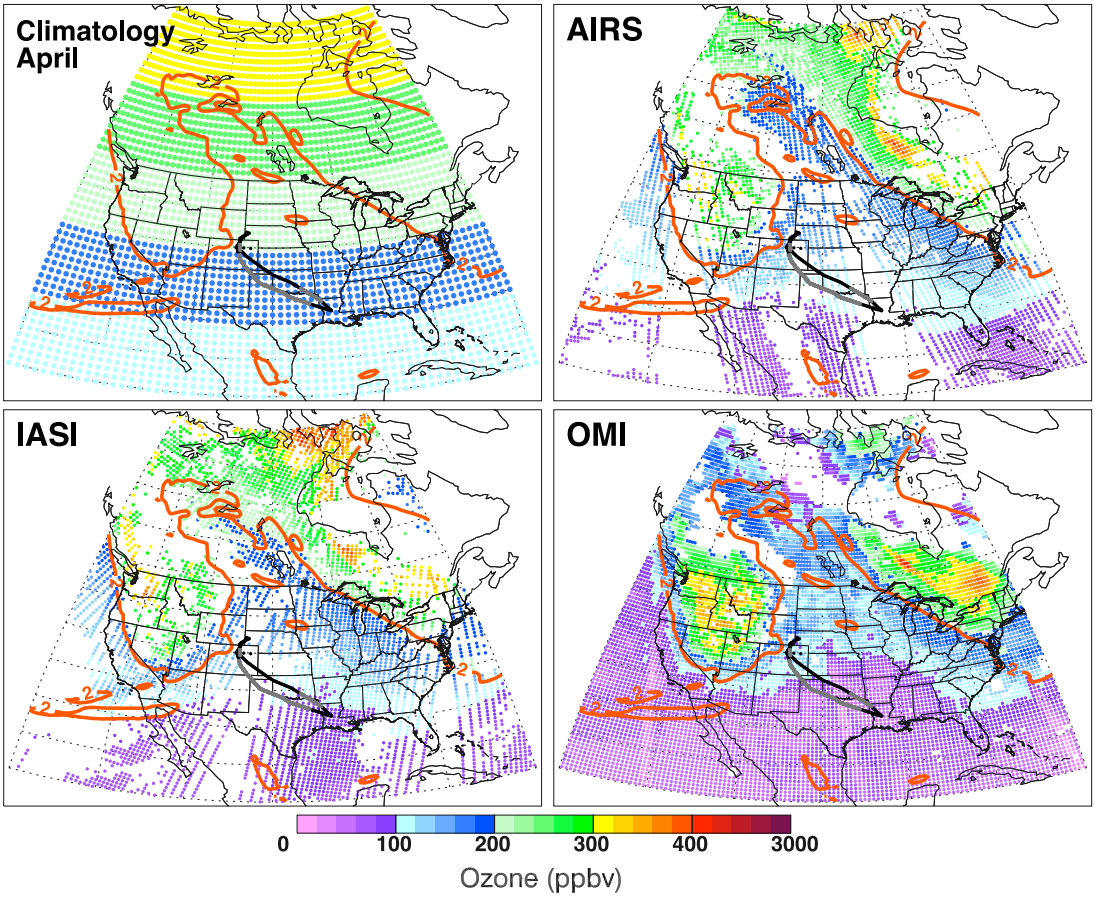

Figure 3. *McPeters et al.* [2007] April climatology used as the first guess in AIRS and IASI and as the a priori in OMI, and ozone retrievals for AIRS, IASI, and OMI in the 212–300 hPa pressure layer for the flight on 30 April 2008. GFS PV = 2 PVU contours derived at 250 hPa are shown in orange. This contour is used as a surrogate for the dynamical tropopause. In addition, the entire flight track is shown in black, with the geographical location of the aircraft while sampling the 212–300 hPa region is shown in gray. Satellite observations with more than 70% cloud fractions are excluded from these plots.

and bottom pressure layers sampled by the aircraft were 2.6 and 2.2 km, respectively. Since the flights were often at constant pressure levels or discrete ascent/descent legs, the aircraft data represent subsamples of the corresponding satellite volumes. Despite these sampling differences, this comparison evaluates how the satellite retrieval products capture the variability and gradients of UTLS ozone observed in Figure 2.

[33] The AIRS and IASI ozone retrievals are screened based on flags similar to the AIRS Version 4 middle tropospheric temperature flags (i.e., Qual_Temp_Profile_Mid; http://disc.sci.gsfc.nasa.gov/AIRS/documentation/documentation/v5_docs/AIRS_V5_Release_User_Docs/V5_L2_Quality_Control_and_Error_Estimation.pdf). Only ozone profiles with middle tropospheric temperature retrieval quality set to "best" are considered. For OMI, different filters are used. Profiles with total measurement area less than 40% of the grid cell area, average radiance fitting residuals greater than 2.0%, and ratio of fitting residuals to OMI random noise errors greater than 1.5 are rejected.

[34] Clouds are not considered for data filtering purposes, except when examining the large-scale dynamic variability in section 4.1. In the horizontal and vertical gradient analyses, cloud information is used to investigate the impact of clouds on the performance of the level 2 satellite retrievals.

[35] Satellite retrievals and aircraft measurements are compared to each other using spatially collocated data. Satellite retrievals are reported at the latitude and longitude of the center of the footprint. In the horizontal gradient analysis, we require the measurements to be within 45 km of each other and to measure continuously for at least 200 km along the flight track to qualify as a valid cruise leg. This horizontal separation is chosen to allow for more opportunities for comparisons. During the campaign, we find a total of 23 cruise legs when all three satellite data are available and 36 cruise legs when only AIRS data are considered. In the vertical gradient analysis, we require the measurements to be within 25 km of each other in horizontal distance regardless of cloud conditions.

4. Results and Discussion

4.1. Dynamic Variability

[36] One of the strengths of the satellite instruments used in this study is their high-density horizontal coverage. Figure 3 shows AIRS, IASI, and OMI ozone fields in the

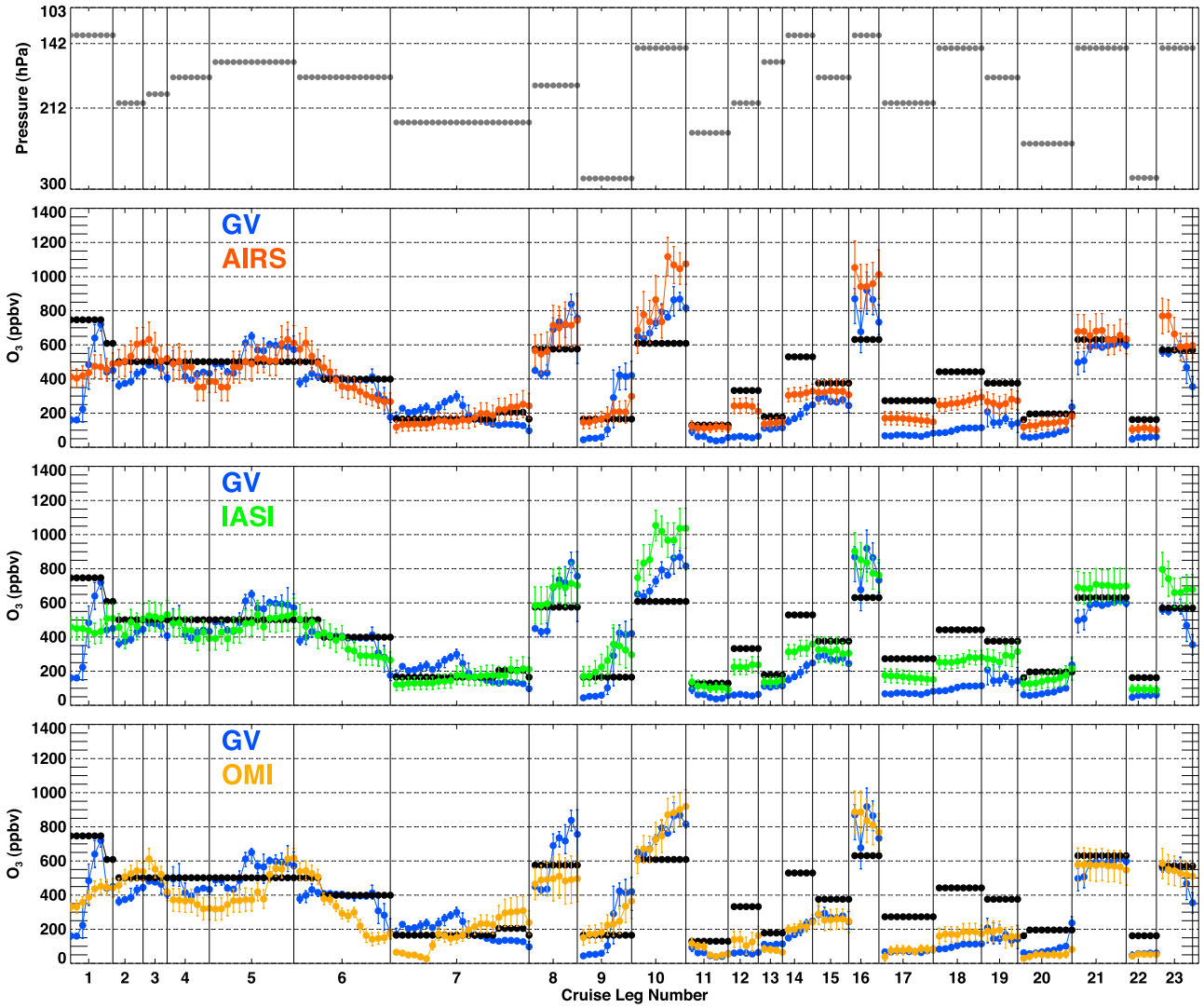

Figure 4. Ozone measurements obtained by the GV aircraft and the satellite instruments while the aircraft flew constant pressure segments during START08. Shown are the 23 cruise legs identified when data from all four instruments were available. Each cruise leg is at least 200 km in length. The black lines correspond to the *McPeters et al.* [2007] climatology used as the first guess in AIRS and IASI and the a priori in OMI. Shown at the top is the ambient pressure during each cruise leg.

212–300 hPa pressure layer over North America on 30 April 2008 and the ozone climatology for the month of April used as a first guess by AIRS and IASI and a priori by OMI. We exclude the cloudiest scenes and consider only retrievals where total cloud fraction is less than 70%.

[37] In addition to ozone fields, Figure 3 also shows the 1800 UT, 250 hPa GFS 2 PV units (1 PVU = 1.0×10^{-6} K m^2 kg^{-1} s^{-1}) contour, which is often used as the dynamical tropopause [*Holton et al.*, 1995]. This contour marks the change from the tropospheric air mass with lower ozone to the stratospheric air mass with higher ozone. Figure 3 shows that all three satellite instruments adequately capture the synoptic-scale ozone gradients associated with strong PV gradients. Such good spatial correlation between ozone and PV is maintained as the large-scale dynamic features evolve over time (not shown). The remarkable positive spatial correlations between ozone and PV as well as the spatially appropriate deviations from the first guess highlight the significant information content in the retrievals.

[38] Ozone-PV spatial correlations over the midlatitudes are very robust. At higher latitudes, AIRS and IASI ozone show expected high ozone magnitudes in areas of high PV. OMI, however, shows negative biases with ozone magnitudes more characteristic of the tropospheric air. This bias has been noted when compared to ozonesondes, and it is likely due to remaining straylight and radiance calculation errors [*Liu et al.*, 2009].

4.2. Horizontal Gradients

[39] In this section, we examine the performance of satellite retrievals when the aircraft sampled horizontal gradients of ozone while flying constant pressure segments or cruise legs. Figure 4 shows a compilation of ambient pressure and ozone obtained by all four instruments over the 23 cruise legs sampled during START08. Also shown are

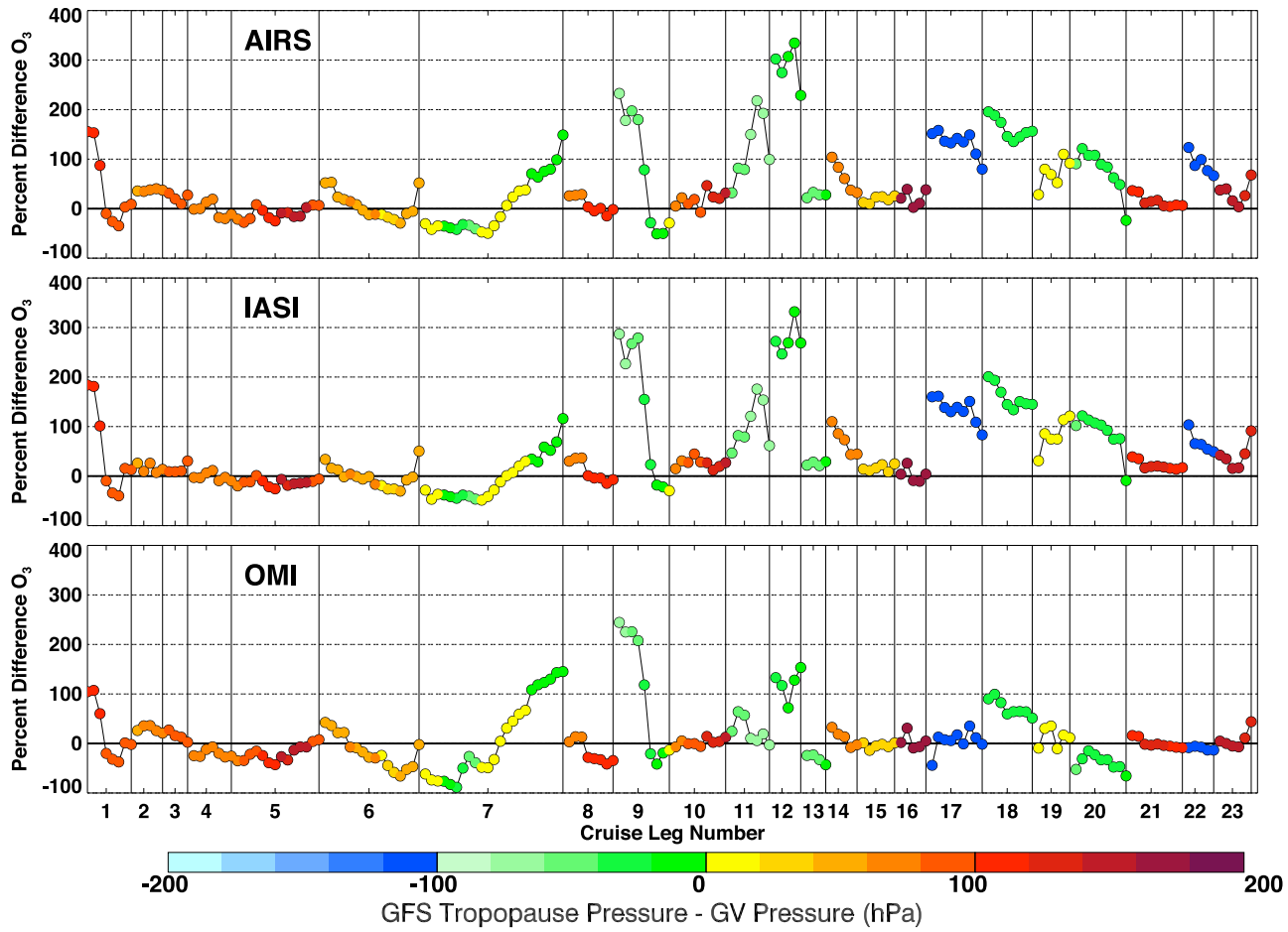

Figure 5. Percent differences between the satellite instruments and the GV aircraft measurements for the same cruise legs shown in Figure 4. Percent difference is defined as (satellite − aircraft)/aircraft × 100. Each data point is colored by the pressure difference between the GFS thermal tropopause and the aircraft location. Yellow and red points are in the stratosphere, and blue and green points are in the troposphere.

the first guess ozone values used in all satellite ozone profile retrievals.

[40] In general, we find that the satellite retrievals have the ability to qualitatively follow the aircraft measurements in the presence of both strong and weak ozone gradients along the cruise legs. In most cases, the retrievals depart from the first guess in the direction of the ozone magnitudes measured by the aircraft instrument. Furthermore, all three satellite instrument retrieval products compare similarly to the aircraft measurements despite the different satellite sampling times and the different measurement techniques used by these three satellite instruments.

[41] Quantitatively, all three satellite instruments often underestimate the magnitude of the horizontal gradient sampled by the aircraft. AIRS and OMI both underestimate the magnitude of the gradient in 56% of the cruise legs by 48% on average, while IASI underestimates the magnitude of the gradient in 78% of the cruise legs by 56% on average.

[42] Owing to the sensitivity of the IR instruments to vertical thermal gradients, we explore the impact that aircraft distance to the GFS-determined thermal tropopause plays on the satellite-aircraft comparisons. Comparisons are performed on a percent basis defined as (satellite-aircraft)/aircraft × 100 in order to normalize differences measured under background conditions that can vary by up to an order of magnitude between the UT and the LS, as seen in Figure 2. Figure 5 shows satellite-aircraft agreements within 50% when the aircraft is sampling the LS, which is furthest away from the tropopause. The largest positive biases, on the order of 100 to 350%, are observed during cruise legs 9, 11, and 12. These cruise legs were flown in the UT, below the tropopause. The results presented in Figure 5 suggest good quantitative agreement between the satellite instruments and the aircraft when the aircraft is in the LS, further away from the tropopause, where ozone variability within the satellite sampling volume is smaller. In the tropopause region, ozone is highly variable and it exhibits large, nonlinear vertical gradients [*Logan*, 1999]. When the aircraft sampled the UT, which is near this region of strong variability and gradients, all three satellite instruments show the largest quantitative disagreements with the aircraft. This result is not surprising considering the chemically different nature of the air masses being compared (i.e., UT by the aircraft versus tropopause region by the satellite).

[43] Next, we explore the relative difference in aircraft and satellite measurements as a function of ozone mixing ratios. The results are shown in Figure 6. For aircraft mixing ratios above 200 parts per billion by volume (ppbv), all

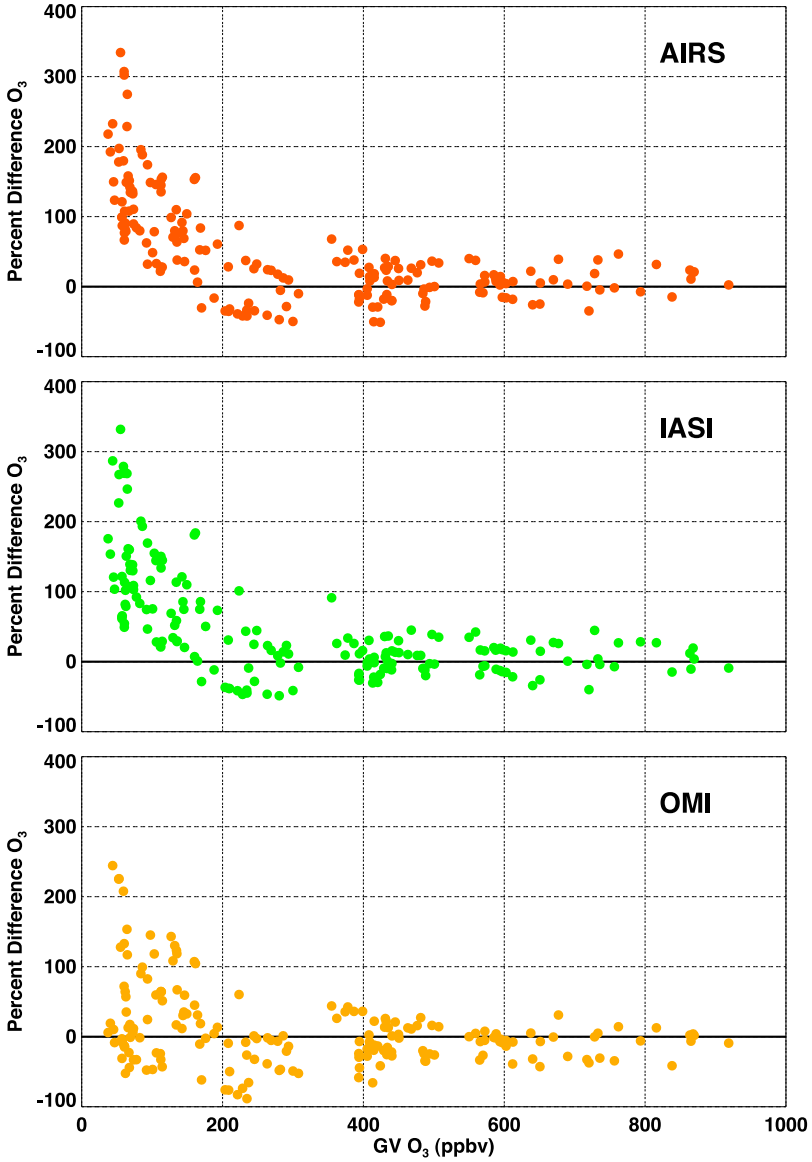

Figure 6. Percent difference between the satellite instruments and the GV aircraft as a function of aircraft ozone using data from the 23 cruise legs shown in Figure 4. Percent difference is defined as (satellite − aircraft)/aircraft × 100.

satellite instruments show agreement with the aircraft within ±50%, for the most part. The largest discrepancies are observed at the aircraft mixing ratios below 200 ppbv. Both AIRS and IASI show increasing positive biases with decreasing ozone, while OMI shows both positive and negative biases at these smaller ozone mixing ratios. Consistent with the results from Figure 5, satellite measurements are most challenged in the UT region where low concentrations, strong gradients and significant variability in ozone exist as evidenced by the START08 aircraft measurements shown in Figure 2.

[44] In order to increase comparison opportunities in the horizontal gradient analysis, we focus on a larger data set that consists of collocated aircraft and AIRS retrievals only. This data set consists of 36 cruise legs. Figure 7 shows scatterplots of aircraft versus AIRS ozone separated by pressure layers and colored by individual cruise legs. We find that AIRS captures the ozone variability throughout the larger range of ozone sampled between 103 and 212 hPa (Figures 7a and 7b). In addition, we find a consistent positive bias at mixing ratios below 300 ppbv over the same pressure range. Between 212 and 300 hPa, however, AIRS shows limited sensitivity to aircraft variability, in particular for aircraft measurements above 200 ppbv.

[45] Given the impact of clouds on IR retrievals, we examine the role that cloud fraction and cloud top pressure play on AIRS retrievals. Figure 8 shows 2-D frequency plots of cloud fraction and cloud top pressure as a function of AIRS and aircraft relative differences during the 36 cruise legs. The majority of the observations reveal that AIRS and aircraft ozone are within ±50% of each other regardless of the percentage of clouds covering the AMSU-A footprint. Similarly, no clear dependence on cloud fraction is found even at the largest AIRS-aircraft discrepancies. While the

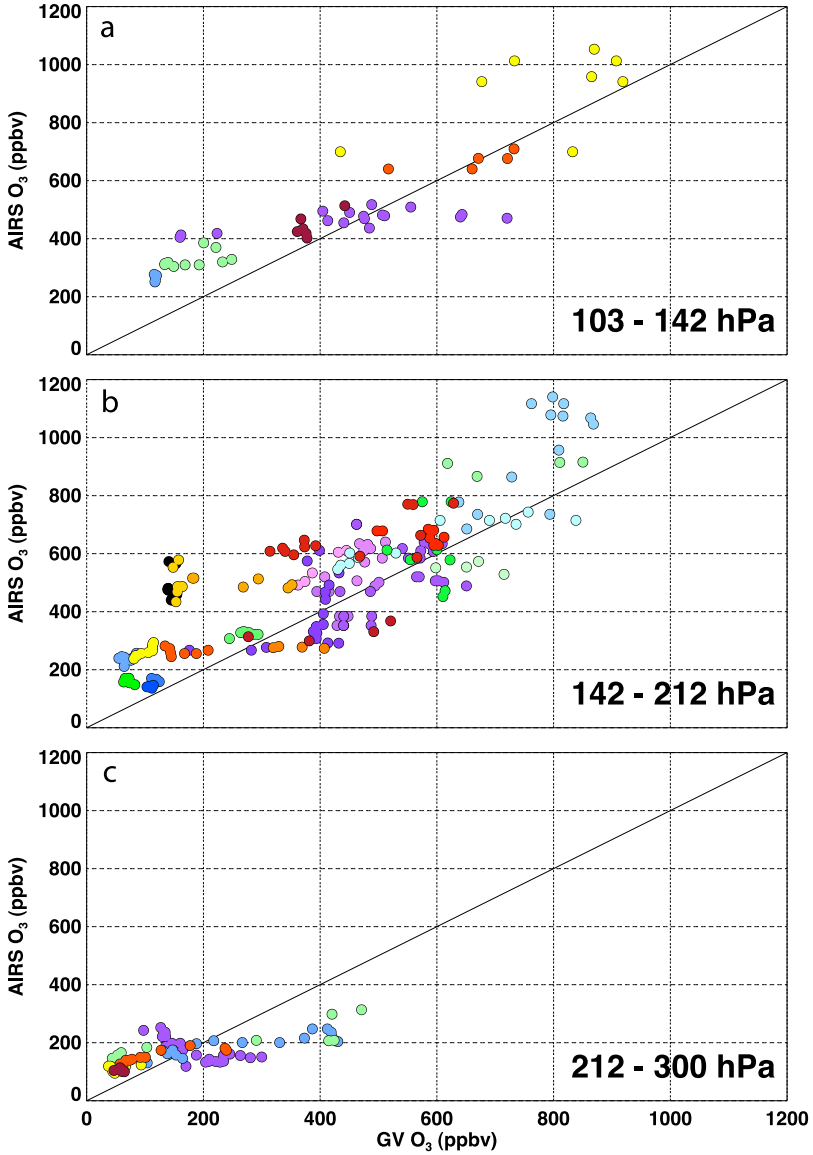

Figure 7. AIRS versus GV aircraft ozone separated by pressure layer and colored differently to distinguish each cruise leg. Shown are the 36 cruise legs identified when aircraft and AIRS data were available. Data point distribution among the UTLS pressure layers is as follows: 16% at 103–142 hPa, 61% at 142–212 hPa, and 23% at 212–300 hPa. The 1:1 line is shown as a visual guide to a perfect correlation.

majority of the AIRS-aircraft comparisons also show agreements within ±50% despite cloud top pressure, we find a tendency for larger ozone discrepancies in the presence of higher cloud tops. If we increase the number of data points by considering all AIRS and aircraft collocated data available during the entire START08 campaign (i.e., both vertical and horizontal flight segments), we find results using the larger data set to be consistent with what is shown in Figure 8.

[46] In order to further evaluate the satellite products and provide insights to the algorithm retrieval teams, we quantify the AIRS retrieval departures from the first guess. Figures 3 and 4 qualitatively show that AIRS, IASI, and OMI have sensitivity in the UTLS as evidenced by departures from the first guess. In Figure 9, we show how much the retrievals depart from the first guess using specific cases represented by aircraft cruise legs. Instead of using absolute magnitudes as shown in Figure 7, we consider percent differences between the retrieval and the first guess, normalized by the first guess. This scale allows us to give equal weight to retrieval–first guess departures despite the magnitude of the background ozone levels. First, we find that the percent departure is comparable in magnitude regardless of pressure layer. Second, we find that for the most part the retrieval tends to decrease the first guess at the lower ozone mixing ratios and increase the first guess at the higher mixing ratios. At the higher pressures, 212 to 300 hPa, we see more scatter in the percent differences at the lower mixing ratios. As previously noted, this layer resides closer to the thermal tropopause where large and nonlinear gradients in ozone are frequently found.

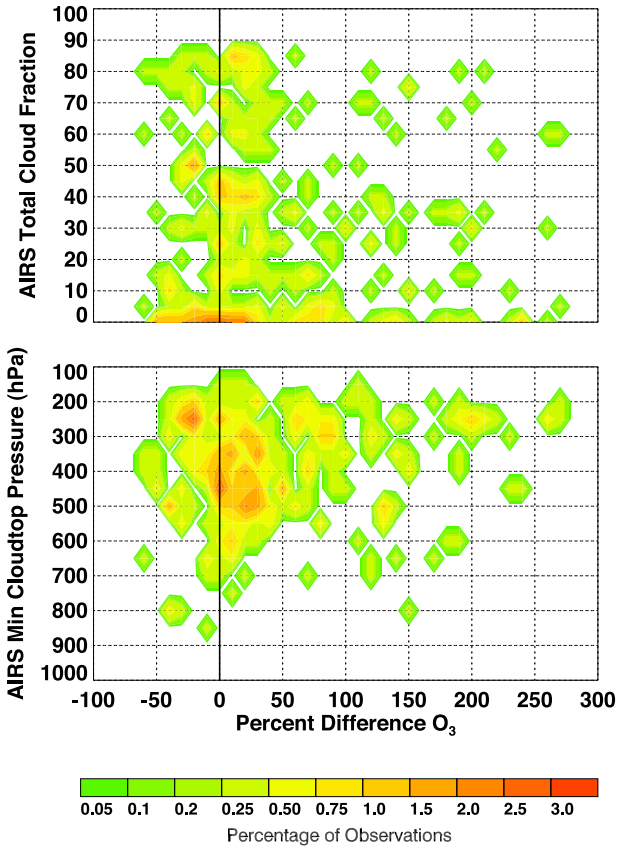

Figure 8. Two-dimensional frequency plots of percent differences in ozone against (top) AIRS total cloud fraction and (bottom) AIRS minimum cloud top pressure during the 36 cruise legs identified when aircraft and AIRS data were available. Percent difference is defined as (AIRS − aircraft)/aircraft × 100.

[47] Analyses equivalent to Figures 7–9 were performed for IASI and OMI (not shown here). The results for IASI are consistent with those obtained for AIRS. Contrary to AIRS and IASI, we find OMI to show higher sensitivity to ozone changes in the 212–300 hPa layer and not to have coincident large positive biases in ozone with the highest cloud tops since UV radiances are not very sensitive to the physical cloud top of optically thin clouds [*Vasilkov et al.*, 2008]. OMI large positive biases coincide with middle level clouds, instead, likely because the effective cloud top pressure is not accurate or because there are broken clouds so the assumption of Lambertian clouds used in the OMI retrievals is no longer valid.

4.3. Vertical Gradients

[48] This section examines how well AIRS, IASI, and OMI capture the troposphere to stratosphere ozone gradients compared to the aircraft observations. We use two different vertical coordinate systems in this analysis. The first one is a relative altitude coordinate system with respect to the GFS thermal tropopause, which emphasizes the location of the sharpest ozone gradient regardless of pressure altitude. Data points are grouped in three chemically different layers: UT, tropopause, and LS. Figure 10 shows median values and 1-sigma variability of absolute ozone mixing ratios for the aircraft and each of the three satellite instruments. Also shown are histograms of ozone mixing ratios sampled by each instrument in each pressure layer. These histograms are specifically shown to illustrate the non-Gaussian character of the data distribution. We choose to show an absolute ozone scale with the relative altitude coordinate because we are examining the ozone gradient across the UTLS using data collected over a large latitudinal range (25° to 65°N) where the tropopause changes in height, so data in the 212–300 hPa layer, for example, would be in the tropopause layer or even in the LS at higher latitudes, but in the UT at lower latitudes.

[49] From a median's perspective, OMI shows the best agreement with the aircraft in the UT and tropopause (+10% and −5% difference, respectively) while AIRS and IASI show the best agreement with the aircraft in the LS (within 1%). In the UT and tropopause, AIRS has an 84 and 15% positive biases, and IASI has an 89 and 26% biases, respectively. It is interesting to note that in this region IASI's slope almost mimics that of the aircraft but with a positive offset. In the LS, OMI shows a negative bias of 21% compared to the aircraft.

[50] The second vertical coordinate system used is actual pressure. Here, data are grouped by pressure layers. Figure 11 shows the relative differences between the satellite instruments and the aircraft for each of the three pressure layers. The comparison is given as the median values and 1-sigma variability of the satellite-aircraft relative differences. To follow commonly found plotting approaches in the literature, we choose to show relative differences with the pressure altitude coordinate. This approach provides averaging for an entire geographical region, neglecting distinction of zonal and/or meridional gradients. The medians of all three instruments agree with the aircraft within ±30%. The variances are within ±50%. OMI shows negative biases of 25%, 22%, and 2% with decreasing pressure. On the contrary, AIRS shows positive biases of 3%, 9%, and 32%, and IASI also shows positive biases but of 28%, 13%, and 20% with decreasing pressure. Similar to Figure 10, we include histograms of the data distribution in each pressure layer. These histograms also show the non-Gaussian nature of the data set. In most cases, the distributions are unimodal with long tails, but in some other cases such as for AIRS at 103–142 hPa the distributions are bimodal.

[51] In addition to the results presented so far, the START08 data set provides the opportunity to statistically quantify the ozone gradients and variability reported in the satellite data compared to those measured by the aircraft. Figure 12 presents least square linear fits of aircraft versus satellite data using (1) all data points in the UTLS and (2) data points from each pressure layer separately. It is interesting to note that all three satellite retrievals show comparable statistical behavior with respect to the aircraft. The best agreement between the satellites and the aircraft occurs at the lowest pressures, which are in general in the LS, furthest away from the tropopause. The slopes of these linear fits are comparable in all three satellite instrument retrievals. These slopes indicate that satellite retrievals underestimate the ozone gradients in the UTLS by 30–40%. This statistical analysis also shows that the satellite retrievals capture more than 80% of the ozone variability in

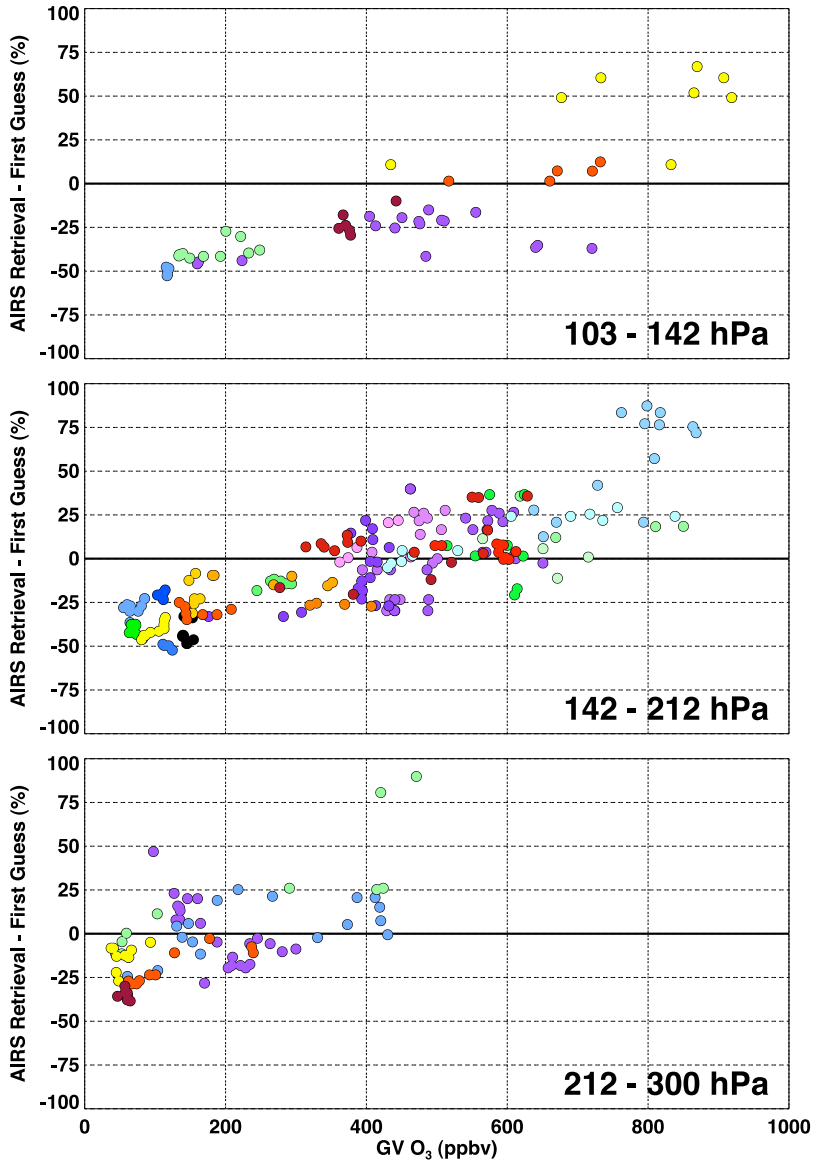

Figure 9. Percent difference between AIRS retrieval and first guess, normalized by the first guess and plotted versus GV aircraft measurements during the 36 cruise legs when aircraft and AIRS data were available. Data points are separated by pressure layers and colored differently to distinguish each cruise leg; the same colors scheme is used as in Figure 7.

the UTLS, with the lowest percentages (58 to 72%), or weaker skills, found in the 212–300 hPa layer.

[52] At lower latitudes, OMI has higher sensitivity to ozone than AIRS and IASI given the nature of the instrument's measurement technique. We explored the possibility of latitude dependence on the least squares linear fits. We find no significant changes in statistical parameters when grouping data points by latitude bins versus pressure bins. These results indicate that satellite-aircraft comparisons are latitude independent within the northern midlatitudes, which is where the START08 data were collected.

[53] We also explored the impact of vertical extent of clouds on statistical relations. Limiting data points to above cloud tops reduces the significance of the statistical results due to a reduction in the number of data points. However, no fundamental differences in the correlations were observed, which indicates that the vertical location of cloud tops does not have a major effect on the satellite-aircraft comparisons.

4.4. Ozone-PV Relationships

[54] Ozone and PV are both stratospheric tracers that have long been used to identify the presence of stratospheric air in the troposphere [*Danielsen*, 1968; *Browell et al.*, 1987]. Early observations showed that these two tracers have a positive correlation near the midlatitude tropopause [*Danielsen*, 1968], which was attributed to similar transport processes regulating their variations [*Allaart et al.*, 1993]. Ozone-PV studies such as *Allaart's et al.* [1993] have focused on maps showing spatial consistency between chemistry (i.e., ozone) and dynamics (i.e., PV), as we showed in Figure 3. Other studies have used the

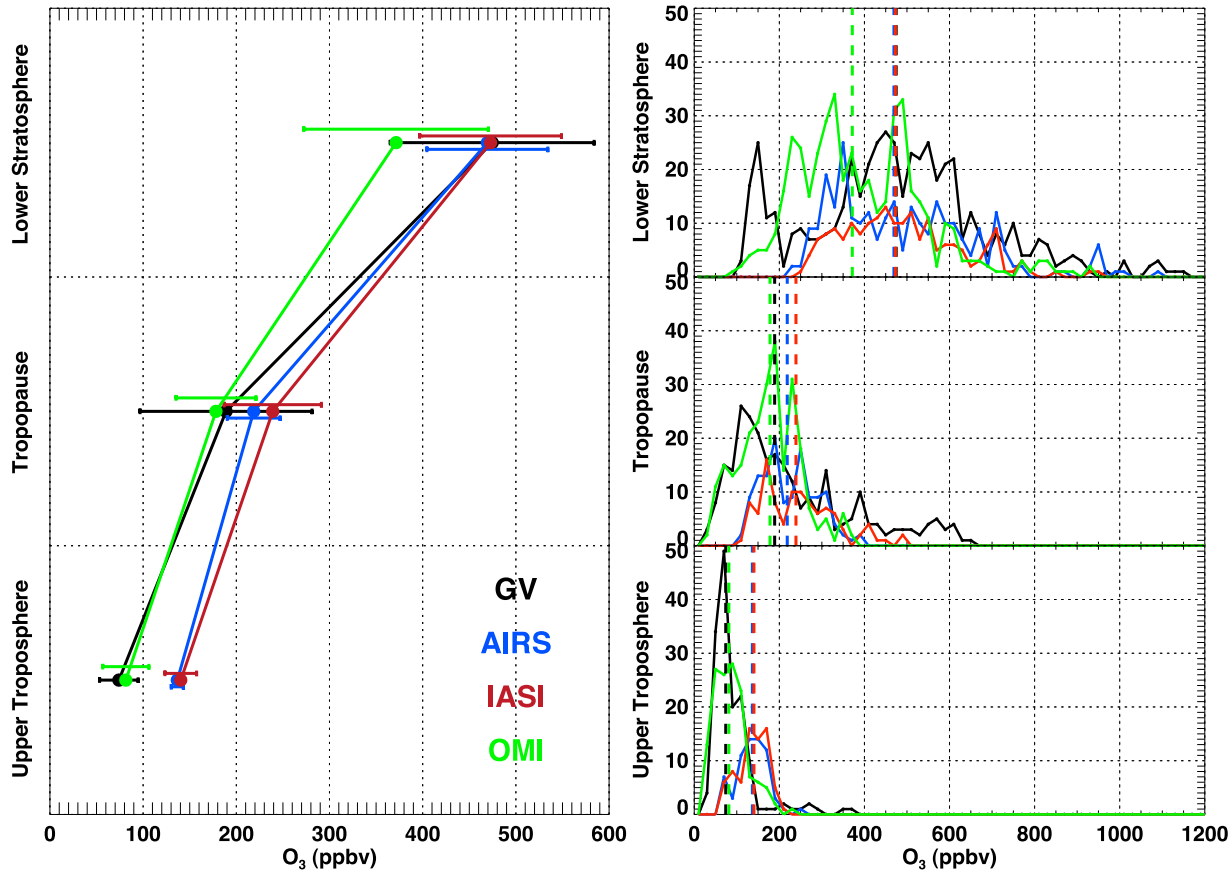

Figure 10. (left) Vertical profiles of ozone from the GV aircraft, AIRS, IASI, and OMI for the START08 campaign constructed using relative height to the GFS thermal tropopause. Values shown are median and 1-sigma variability. Variability bars are offset in the vertical for better visualization of the ranges. (right) Histograms of the measurements used to determine the median value in each pressure layer. The dashed vertical lines correspond to the median values for each instrument.

ozone-PV relation to identify [*Newell et al.*, 1997] and derive [*Browell et al.*, 2003a; *Browell et al.*, 2003b] stratospheric influence of air in the UT as well as infer ozone magnitudes in the polar vortex in the absence of ozone measurements [*Randall et al.*, 2002]. Recent aircraft measurements obtained over Europe during the SPURT campaign have shown that the ozone-PV relation in the UTLS has a seasonal dependence, with higher ozone mixing ratios observed at any given PVU during the springtime as a result of enhanced downward motion from the LS [*Krebsbach et al.*, 2006]. In this section, our goal is to evaluate the capabilities of the satellite ozone retrievals to reproduce the ozone-PV relation observed in the aircraft data.

[55] To this end, we compare collocated aircraft and satellite retrievals as a function of PV fields interpolated to the aircraft flight track. The results are shown in Figure 13 as 2-D frequency plots that include data from the entire START08 campaign. Also shown in the figure are least square linear fits in the 0–5 PVU range, nominally the region that includes the UTLS.

[56] We find that all three satellite retrievals are able to reproduce the general shape of the ozone-PV relation observed by the aircraft: two distinct slopes at low and high PVUs, with a smaller variance at the low PVUs (less than 5 PVU) compared to the high PVUs (more than 5 PVU). Furthermore, ozone-PV gradients in the UTLS are captured by all satellite retrievals to within ±23% of the aircraft's. Consistent with the results shown in Figures 10 and 11, AIRS and IASI show a larger positive bias in the ozone-PV relation in the UTLS compared to OMI.

5. Conclusions

[57] We have presented a set of analyses to evaluate the AIRS, IASI, and OMI ozone profile retrievals in the UTLS using aircraft measurements from the START08 campaign. Although the data set has limited spatial coverage, the comparison serves to evaluate the ozone retrievals under a variety of conditions ranging from weak to strong gradients both in the horizontal and in the vertical. Overall, we found that AIRS, IASI, and OMI show consistent behavior among each other and all three instrument retrievals compare similarly to the aircraft data.

[58] The analysis presented in this study elucidated the good capabilities AIRS, IASI, and OMI retrievals have in capturing synoptic-scale ozone gradients associated with strong PV gradients. Furthermore, we found that the retrieved ozone features maintain good spatial correlation with PV over time. This capability can be attributed to the significant information content that these measurements

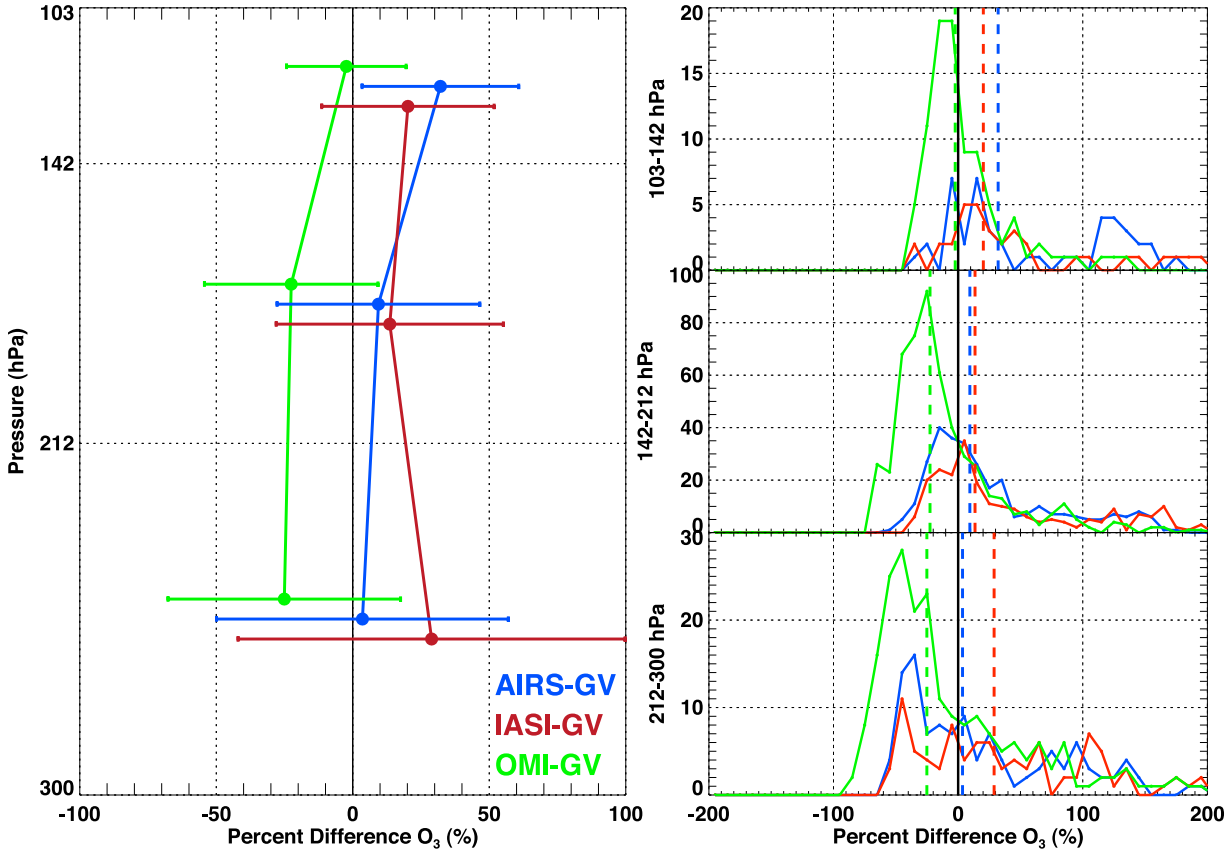

Figure 11. (left) Percent differences between the satellite instruments and the GV aircraft as a function of pressure layer for the START08 campaign. Values shown are median and 1-sigma variability. Variability bars are offset in the vertical for better visualization of the ranges. Percent difference is defined as (satellite − aircraft)/aircraft × 100. (right) Histograms of percent differences showing the distribution of points used in the calculation of the median values. The dashed vertical lines correspond to the median values. Note the different y scale used in each pressure layer.

have due to their high horizontal resolution and coverage. The excellent dynamic variability captured by the satellite retrievals indicates that these data sets can be used to provide large-scale context for in situ measurements, such as aircraft and ozonesondes.

[59] From a qualitative point of view, all satellite instruments showed good sensitivity to both weak and strong horizontal gradients in ozone. From a quantitative point of view, we found that satellite-aircraft discrepancies were influenced by the location of the sampling volume with respect to the thermal tropopause, and thus the chemical nature of such volume. For instance, satellite measurements agree with the aircraft within ±50% in the LS, where ozone fields are greater than 200 ppbv and the volumes sampled are more homogeneous. In the tropopause region, however, large differences between aircraft and satellite measurements are often observed. AIRS and IASI have consistent positive biases with respect to the aircraft, while OMI has both positive and negative biases. Ozone in this region is highly variable, and detection of small-scale features such as those sampled by the aircraft are challenging to resolve by the satellite instruments given their broader vertical resolution.

[60] We also found that clouds have an effect on the IR retrievals examined in this study. The largest IR satellite-aircraft biases in ozone were found in the presence of the highest cloud tops.

[61] All three satellite retrievals capture the vertical gradients in ozone in the UTLS region. Quantitative comparisons to the aircraft measurements indicated negative biases in OMI ranging from 2 to 25%, and positive biases in AIRS and IASI ranging from 3 to 30% in the UTLS. When using a tropopause based vertical coordinate, we found OMI to match the aircraft to within 10% in the UT and tropopause regions, but to underestimate the amount of ozone in the LS by 22%. AIRS and IASI, on the contrary, were 15 to 90% higher than the aircraft in the UT and tropopause regions, but within 1% in the LS. Despite the partial coverage of the 103–142 hPa layer by the aircraft, our analysis showed median biases to be within ±30%, comparable to the results obtained in the 142–212 hPa layer, which was fully sampled by the aircraft (see Figure 11).

[62] All three satellite retrievals also show good capabilities to capture ozone variability in the UTLS. Statistical analyses showed that the satellite retrievals capture ∼80% of the ozone variability observed in the aircraft data. The lowest sensitivity to gradients and variability in ozone are found in the 212–300 hPa layer, with OMI showing higher sensitivity than AIRS and IASI at these pressures.

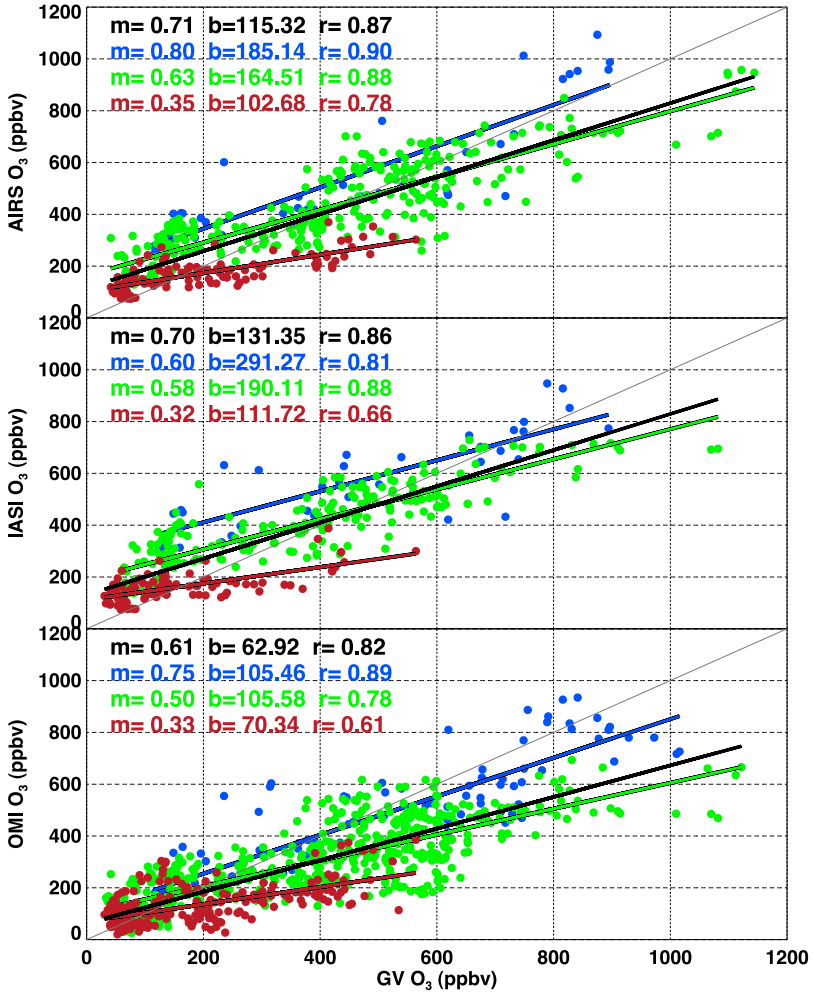

Figure 12. Satellite versus GV aircraft correlation plots of ozone for the START08 campaign, for (top) AIRS, (middle) IASI, and (bottom) OMI. The data points are separated based on pressure layers: 103 to 142 hPa (blue), 142 to 212 hPa (green), and 212 to 300 hPa (red). Also shown are slope (m), intercept (b), and correlation coefficients (r) obtained from linear fits to the data. These statistics are calculated for (1) all UTLS data points (black) and (2) each pressure layer separately (colors).

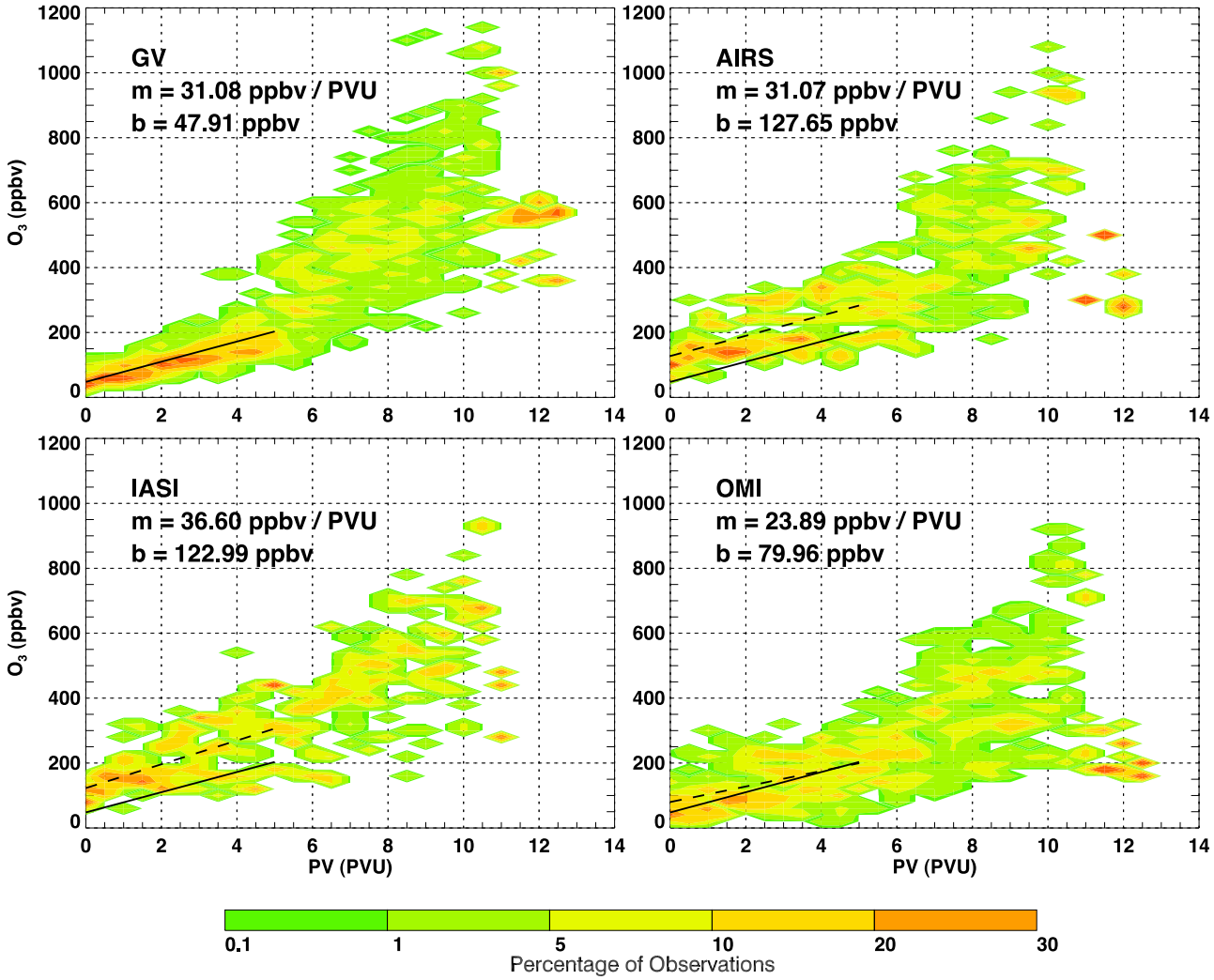

Figure 13. Two-dimensional frequency plots of ozone-PV relations for the START08 campaign. Satellite data are spatially collocated with the GV aircraft. GFS PV is calculated along the flight track. A linear fit to the data from 0 to 5 PVU, which includes the UTLS region, is shown. The solid line represents the linear fit to the aircraft data set, and the dashed lines represent the linear fit to each satellite data set.

[63] The START08 data set also provided the opportunity to compare ozone-PV relations along the flight track. We found the satellite instruments to capture the general shape of the relation and to reproduce the gradients in the 0–5 PVU region to within ±23% of the aircraft's.

[64] Given that the UTLS plays a significant role in chemistry-climate interactions, and few satellite instruments provide continuous global daily coverage that adequately map the synoptic scale ozone variability, the three satellite data sets evaluated in this work represent significant asset for climate relevant process studies. Characterizations of these data sets and continued improvement of retrieval techniques will benefit not only the existing data sets, but also future data from upcoming satellite instruments of similar capabilities, which include Cross-track Infrared Sounder (CrIS) soon to be launched on the U. S. National Polar-orbiting Operational Environmental Satellite System (NPOESS), and future IASI instruments on MetOp-B and MetOp-C.

[65] **Acknowledgments.** The National Center for Atmospheric Research is sponsored by the National Science Foundation. This work is partially supported by the AIRS project. The authors would like to thank the reviewers for very helpful comments that contributed to the improvement of this manuscript. In addition, gratitude is also extended to START08 team for the aircraft data.

References

Acarreta, J. R., J. F. De Haan, and P. Stammes (2004), Cloud pressure retrieval using the O_2-O_2 absorption band at 477 nm, *J. Geophys. Res.*, *109*, D05204, doi:10.1029/2003JD003915.

Allaart, M. A. F., H. Kelder, and L. C. Heijboer (1993), On the relation between ozone and potential vorticity, *Geophys. Res. Lett.*, *20*(9), 811–814, doi:10.1029/93GL00822.

Aumann, H. H., et al. (2003), AIRS/AMSU/HSB on the Aqua mission: Design, science objectives, data products, and processing systems, *IEEE Trans. Geosci. Remote Sens.*, *41*, 2, doi:10.1109/TGRS.2002.808356.

Bian, J., A. Gettelman, H. Chen, and L. L. Pan (2007), Validation of satellite ozone profile retrievals using Beijing ozonesonde data, *J. Geophys. Res.*, *112*, D06305, doi:10.1029/2006JD007502.

Browell, E. V., E. F. Danielsen, S. Ismail, G. L. Gregory, and S. M. Beck (1987), Tropopause fold structure determined from airborne lidar and in situ measurements, *J. Geophys. Res.*, *92*(D2), 2112–2120, doi:10.1029/JD092iD02p02112.

Browell, E. V., et al. (2003a), Ozone, aerosol, potential vorticity, and trace gas trends observed at high-latitudes over North America from February to May 2000, *J. Geophys. Res.*, *108*(D4), 8369, doi:10.1029/2001JD001390.

Browell, E. V., et al. (2003b), Large-scale ozone and aerosol distributions, air mass characteristics, and ozone fluxes over the western Pacific Ocean in late winter/early spring, *J. Geophys. Res.*, *108*(D20), 8805, doi:10.1029/2002JD003290.

Chahine, M. T. (1968), Determination of the temperature profile in an atmosphere from its outgoing radiance, *J. Opt. Soc. Am.*, *58*, 1634–1637, doi:10.1364/JOSA.58.001634.

Chahine, M. T., L. Chen, P. Dimotakis, X. Jiang, Q. Li, E. T. Olsen, T. Pagano, J. Randerson, and Y. L. Yung (2008), Satellite remote sounding of mid-tropospheric CO2, *Geophys. Res. Lett.*, *35*, L17807, doi:10.1029/2008GL035022.

Clerbaux, C., et al. (2007), The IASI/MetOp I mission: First observations and highlights of its potential contribution to GMES, *Space Res. Today*, *168*, 19–24, doi:10.1016/S0045-8732(07)80046-5.

Danielsen, E. F. (1968), Stratosphere-tropospheric exchange based on radioactivity, ozone and potential vorticity, *J. Atmos. Sci.*, *25*, 502–518, doi:10.1175/1520-0469(1968)025<0502:STEBOR>2.0.CO;2.

Divakarla, M., et al. (2008), Evaluation of Atmospheric Infrared Sounder ozone profiles and total ozone retrievals with matched ozonesonde measurements, ECMWF ozone data, and Ozone Monitoring Instrument retrievals, *J. Geophys. Res.*, *113*, D15308, doi:10.1029/2007JD009317.

Gettelman, A., P. M. de F. Forster, M. Fujiwara, Q. Fu, H. Vömel, L. K. Gohar, C. Johanson, and M. Ammerman (2004), Radiation balance of the tropical tropopause layer, *J. Geophys. Res.*, *109*, D07103, doi:10.1029/2003JD004190.

Holton, J. R., P. H. Haynes, M. E. McIntyre, A. R. Douglass, R. B. Rood, and L. Pfister (1995), Stratosphere-troposphere exchange, *Rev. Geophys.*, *33*(4), 403–439, doi:10.1029/95RG02097.

Kirk-Davidoff, D. B., J. G. Anderson, E. J. Hintsa, and D. W. Keith (1999), The effect of climate change on ozone depletion through stratospheric water vapor, *Nature*, *402*, 399–402, doi:10.1038/46521.

Krebsbach, M., et al. (2006), Seasonal cycles and variability of O3 and H2O in the UT/LMS during SPURT, *Atmos. Chem. Phys.*, *6*, 109–125.

Levelt, P. F., et al. (2006), The Ozone Monitoring Instrument, *IEEE Trans. Geosci. Remote Sens.*, *44*, 1093–1101, doi:10.1109/TGRS.2006.872333.

Liu, X., et al. (2005), Ozone profile and tropospheric ozone retrievals from Global Ozone Monitoring Experiment: Algorithm description and validation, *J. Geophys. Res.*, *110*, D20307, doi:10.1029/2005JD006240.

Liu, X., P. K. Bhartia, K. Chance, R. J. D. Spurr, and T. P. Kurosu (2009), Ozone profile retrievals from the Ozone Monitoring Instrument, *Atmos. Chem. Phys. Disc.*, *9*, 22,693–22,738.

Logan, J. A. (1999), An analysis of ozonesonde data for the lower stratosphere: Recommendations for testing models, *J. Geophys. Res.*, *104*(D13), 16,151–16,170, doi:10.1029/1999JD900216.

Logan, J. A., et al. (1999), Trends in the vertical distribution of ozone: A comparison of two analyses of ozonesonde data, *J. Geophys. Res.*, *104*(D21), 26,373–26,399, doi:10.1029/1999JD900300.

Maddy, E. S., and C. D. Barnet (2008), Vertical resolution estimates in Version 5 of AIRS operational retrievals, *IEEE Trans. Geosci. Remote Sens.*, *46*, 8, doi:10.1109/TGRS.2008.917498.

Maddy, E. S., C. D. Barnet, M. Goldberg, C. Sweeney, and X. Liu (2008), CO2 retrievals from the Atmospheric Infrared Sounder: Methodology and validation, *J. Geophys. Res.*, *113*, D11301, doi:10.1029/2007JD009402.

McMillan, W. W., C. Barnet, L. Strow, M. T. Chahine, M. L. McCourt, J. X. Warner, P. C. Novelli, S. Korontzi, E. S. Maddy, and S. Datta (2005), Daily global maps of carbon monoxide from NASA's Atmospheric Infrared Sounder, *Geophys. Res. Lett.*, *32*, L11801, doi:10.1029/2004GL021821.

McPeters, R. D., G. J. Labow, and J. A. Logan (2007), Ozone climatological profiles for satellite retrieval algorithms, *J. Geophys. Res.*, *112*, D05308, doi:10.1029/2005JD006823.

Monahan, K. P., L. L. Pan, A. J. McDonald, G. E. Bodeker, J. Wei, S. E. George, C. D. Barnet, and E. Maddy (2007), Validation of AIRS v4 ozone profiles in the UTLS using ozonesondes from Lauder, NZ and Boulder, USA, *J. Geophys. Res.*, *112*, D17304, doi:10.1029/2006JD008181.

Newell, R. E., E. V. Browell, D. D. Davis, and S. C. Liu (1997), Western Pacific tropospheric ozone and potential vorticity: Implications for Asian pollution, *Geophys. Res. Lett.*, *24*(22), 2733–2736, doi:10.1029/97GL02799.

Pan, L. L., et al. (2007), Chemical behavior of the tropopause observed during the Stratosphere-Troposphere Analyses of Regional Transport (START) experiment, *J. Geophys. Res.*, *112*, D18110, doi:10.1029/2007JD008645.

Pan, L. L., K. P. Bowman, E. Atlas, S. C. Wofsy, F. Zhang, J. Bresch, J. V. Pittman, C. Homeyer, W. Cooper, and P. Romashkin (2009), Stratosphere-troposphere analyses of regional transport experiment, *Bull. Am. Meteorol. Soc.*, in press.

Proffitt, M. H., and R. J. McLaughlin (1983), Fast-response dual-beam UV absorption ozone photometer suitable for use on stratospheric balloons, *Rev. Sci. Instrum.*, *54*, 1719–1728, doi:10.1063/1.1137316.

Randall, C. E., et al. (2002), Reconstruction of three-dimensional ozone fields using POAM III during SOLVE, *J. Geophys. Res.*, *107*(D20), 8299, doi:10.1029/2001JD000471.

Smith, J. B., E. J. Hintsa, N. T. Allen, R. M. Stimpfle, and J. G. Anderson (2001), Mechanisms for midlatitude ozone loss: Heterogeneous chemistry in the lowermost stratosphere?, *J. Geophys. Res.*, *106*(D1), 1297–1309, doi:10.1029/2000JD900464.

Sneep, M., J. F. de Haan, P. Stammes, P. Wang, C. Vanbauce, J. Joiner, A. P. Vasilkov, and P. F. Levelt (2008), Three-way comparison between OMI and PARASOL cloud pressure products, *J. Geophys. Res.*, *113*, D15S23, doi:10.1029/2007JD008694.

Spurr, R. (2003), LIDORT V2PLUS: A comprehensive radiative transfer package for UV/VIS/NIR nadir remote sensing: A general quasi analytic solution, *Proc. SPIE*, *5235*, 89–100.

Strow, L. L., et al. (2003), An overview of the AIRS radiative transfer model, *IEEE Trans. Geosci. Remote Sens.*, *41*, 2, doi:10.1109/TGRS.2002.808244.

Susskind, J., C. D. Barnet, and J. M. Blaisdell (2003), Retrieval of atmospheric and surface parameters from AIRS/AMSU/HSB data in the presence of clouds, *IEEE Trans. Geosci. Remote Sens.*, *41*, 2, doi:10.1109/TGRS.2002.808236.

Vasilkov, A., J. Joiner, R. Spurr, P. K. Bhartia, P. Levelt, and G. Stephens (2008), Evaluation of the OMI cloud pressures derived from rotational Raman scattering by comparisons with other satellite data and radiative transfer simulations, *J. Geophys. Res.*, *113*, D15S19, doi:10.1029/2007JD008689.

Xie, F., W. Tian, and M. P. Chipperfield (2008), Radiative effect of ozone change on stratosphere-troposphere exchange, *J. Geophys. Res.*, *113*, D00B09, doi:10.1029/2008JD009829.

Xiong, X., C. Barnet, E. Maddy, C. Sweeney, X. Liu, L. Zhou, and M. Goldberg (2008), Characterization and validation of methane products from the Atmospheric Infrared Sounder (AIRS), *J. Geophys. Res.*, *113*, G00A01, doi:10.1029/2007JG000500.

Xiong, X., S. Houweling, J. Wei, E. Maddy, F. Sun, and C. Barnet (2009), Methane plume over South Asia during the monsoon season: Satellite observation and model simulation, *Atmos. Chem. Phys.*, *9*, 783–794.

Yurganov, L. N., W. W. McMillan, A. V. Dzhola, E. I. Grechko, N. B. Jones, and G. R. van der Werf (2008), Global AIRS and MOPITT CO measurements: Validation, comparison, and links to biomass burning variations and carbon cycle, *J. Geophys. Res.*, *113*, D09301, doi:10.1029/2007JD009229.

C. D. Barnet, Center for Satellite Application and Research, National Environmental Satellite, Data, and Information Service, NOAA, Camp Springs, MD 20746, USA.

K. Chance, Harvard-Smithsonian Center for Astrophysics, Cambridge, MA 02138, USA.

R.-S. Gao, National Oceanographic and Atmospheric Administration, Boulder, CO 80305, USA.

F. W. Irion, Jet Propulsion Laboratory, California Institute of Technology, Pasadena, CA 91109, USA.

X. Liu, Goddard Earth Sciences and Technology Center, University of Maryland Baltimore County, Baltimore, MD 20771, USA.

E. S. Maddy and J. C. Wei, Perot Systems Government Services, Fairfax, VA 22031, USA.

L. L. Pan and J. V. Pittman, National Center for Atmospheric Research, Boulder, CO 80301, USA. (pittman@ucar.edu)